Quantum Electronics **51** (5) 423–426 (2021)

https://doi.org/10.1070/QEL17544

Diode laser generating 3-ns pulses for a high resolution lidar

S.M. Pershin, M.Ya. Grishin, V.A. Zavozin, V.S. Makarov,
V.N. Lednev, A.N. Fedorov, A.V. Myasnikov, A.V. Turin

Abstract. **An AlGaAs laser (907 nm, 0.2 μJ) with a 3-ns pulse duration and eye-safe energy density below 1 μJ cm^{-2} is developed for lidar application. The laser is composed of three stacked diodes in a plastic housing. An external pump current generator based on discrete elements with an FMMT417 bipolar transistor switch is assembled on a printed circuit board together with the laser. A lidar based on this laser and a single photon avalanche diode (SPAD) as a detector is used to monitor aerosols with a resolution of 10 cm inside the tunnel of the Baksan Neutrino Observatory near the Elbrus volcano. An abrupt three-fold increase in aerosol emanation of yet unknown nature is recorded for the first time. The absence of the Earth's crust disturbance traces in the signal of a laser interferometer with a resolution of 1.6×10^{-11} m testifies to a high sensitivity of the lidar for monitoring geodynamic processes.**

Keywords: *diode laser, lidar, magmatic gases, Earth's crust deformation, monitoring of geophysical processes.*

1. Introduction

It is known [1–5] that a decrease in the laser pulse duration is a necessary condition for increasing the resolution of lidars. At the same time, the main restriction of using pulsed lidars for ecosystem monitoring is that visible laser radiation with energy densities exceeding 1 μJ cm^{-2} is dangerous for human eyes [6].

In this connection, we proposed for the first time, to our knowledge, to design a lidar system using a diode laser and a detector based on a single-photon avalanche photodiode (SPAD) [8]. Gating of the detector by a short pulse made it possible to efficiently (by several orders of magnitude) suppress the background noise. Taking these features into account, we proposed a new, purely statistical principle of lidar sensing by microjoule (eye-safe) diode laser pulses [7, 9–12], when the probability of detecting probe pulse photons scattered along the track is less than unity [9]. It is known that diode lasers are characterised by high efficiency and compactness, but a decrease in the pulse duration from 120 ns [7] to several nanoseconds [13–17] remains an actual problem [1–5] for, e.g., increasing the range resolution of lidars.

Our first lidar system was assembled [7] on the basis of an LPI-102 AlGaAs diode laser (OAO Voskhod) (τ = 120 ns, pulse energy ~0.5 μJ, wavelength 880 nm, pulse repetition rate 2.5 kHz) and a SPAD [8] with a low avalanche breakdown voltage (27 V). Despite the low, eye-safe energy density (below 1 μJ cm^{-2}), this lidar can sense clouds and plumes at a distance of thousands of meters with a step of 5 m [10]. For example, multi-layered clouds near the Elbrus volcano summit were detected at a distance exceeding 4000 m [11]. The high efficiency and noise immunity of the lidar, its small weight, and ability to operate at a temperature of 100 °C allowed us to win the NASA international competition [13] for participation in the NASA mission 'Mars Polar Lander-99' [14].

Recently, we have detected (for the first time) the Earth's crust deformation by measuring the variation in aerosol concentration inside a short (17 m) laser strainmeter tunnel [15]. Symbatic changes in the lidar signal and the length of the measuring shoulder of the Michelson interferometer showed that the lidar is a new instrument for monitoring geodynamic processes. However, the large pulse duration of the LPI-102 laser (120 ns) and the large spatial discretisation step (5 m) did not allow us to detect local aerosol emanations and to measure the profile of their distribution along the short tunnel.

The aim of the present work was to reduce the diode laser pulse duration to increase the lidar resolution.

The possibility of generating nanosecond pulses by laser diodes was demonstrated in works [16–20]. It was shown that, to decrease the laser pulse duration, it is necessary to increase the discharge current commutation rate and decrease the losses, capacitance, and inductance of the pulsed power supply circuit of the laser. For this purpose, the authors of [15, 17] developed a technology of integrating the layers and elements of the capacitive discharge circuit in the thyristor heterostructure. However, the possibility of decreasing the pulse duration of a diode laser with a current generator based on commercially produced discrete elements remained unclear.

2. Experiment and measurement results

As a source of short pulses, we chose an SPL PL90_3 laser (OSRAM) composed of three stacked AlGaAs diodes in a plastic housing without an integrated current generator. This laser was chosen because summing of the energies of three diodes ensures: (1) simultaneous pumping of all three diodes

S.M. Pershin, M.Ya. Grishin, V.A. Zavozin, V.N. Lednev, A.N. Fedorov Prokhorov General Physics Institute, Russian Academy of Sciences, ul. Vavilova 38, 119991 Moscow, Russia;
e-mail: pershin@kapella.gpi.ru;
V.S. Makarov, A.V. Turin Space Research Institute, Russian Academy of Sciences, ul. Profsoyuznaya 84/32, 117133 Moscow, Russia;
A.V. Myasnikov Sternberg Astronomical Institute, Moscow State University, Universitetskii prosp. 13, 119234 Moscow, Russia

Received 26 February 2021
Kvantovaya Elektronika **51** (5) 423–426 (2021)
Translated by M.N. Basieva

without current branching as in the LPI-102 laser [7]; (2) minimum capacitance; (3) minimum size of the emitting region (200 × 10 μm), which is important for decreasing the beam divergence (3 × 0.15 mrad) at the given focal length (70 mm) and aperture (15 × 40 mm) of the lidar lens; and (4) a common power supply for the laser and the single-photon avalanche photodiode due to the use of an external discharge current generator. Note that LPI-102 lasers with integrated generators [7] require two separate power supply units, which complicates the scheme and increases the overall dimensions and weight of the lidar.

For laser pumping, we developed a repetitively pulsed generator of short current pulses (2–20 ns), the end part of which with a laser diode LD is shown in Fig. 1a. To decrease the current pulse duration, we used a fast FMMT417 bipolar transistor T with a working voltage of up to 300 V to switch the storage capacitor C1 (82 pF). The transistor operates in the avalanche regime; starting pulses from the current generator are applied to the transistor base with the required pulse repetition rate of the lidar (in our case, 10 kHz). After switching off the transistor T, the capacitor C1 is charged through resistors R1 and R2. The high voltage +HV is selected in the process of generator adjustment for each capacitance of the capacitor C1. The decrease in the laser pulse duration to 4 ns (see the oscillogram in Fig. 1b) is achieved by increasing the voltage +HV and decreasing the C1 capacitance.

The physical processes and the operation algorithm of the lidar with the SPAD operating in the Geiger regime are analysed in detail in [9]. Note that the progress in the development of specialised time-to-digital converter microchips allowed us to decrease the track discretisation step almost by two orders of magnitude, i.e., from 5 [7, 9–12] to 0.1 m, by using an ACAM TDC-GP1 series microchips. As will be shown below, this discretisation step increases the spatial resolution and allows measurement of the envelope of optical pulses with a duration exceeding 1 ns.

After assembling and adjusting the lidar with a single-photon avalanche photodiode, we performed test measurements in a corridor of the building of the General Physics Institute. Figure 1c shows the lidar signal in the case of measuring the distance to a flat wall at the end of the sensing track with a discretisation step of 10 cm and 50000 triggering laser pulses. One can see that the shape of lidar signal envelope with a short front and a prolonged trailing edge is asymmetric, as well as the pulse shape on the oscillogram (Fig. 1b). This shape of pulses is characteristic for diode lasers pumped by a capacitor discharge current [16–19]. Note that the laser pulse duration (~2.7 ns) at half maximum of the histogram of lidar photocounts from a flat wall (Fig. 1c) is smaller than that of the oscilloscope pulse (Fig. 1b). The increase in the pulse duration on the oscillogram to 4 ns is caused by the relatively narrow bandwidth of the used Aktakom ADS-2332 oscilloscope (300 MHz). At a voltage of 300 V and a C1 capacitance of 82 pF, the laser pulse energy was 0.2 μJ. The width of the laser spectrum was 7 nm, the power/temperature coefficient was 0.4% $°C^{-1}$, and the wavelength/temperature coefficient was 0.28 nm $°C^{-1}$.

One can see from Fig. 1c that the lidar can act as an oscilloscope with a bandwidth of several GHz and digitise nanosecond optical pulses. It is clear that the use of other time-to-digital converters that provide a discretisation step of 5–10 mm, makes it possible to use the lidar for measuring the envelope of optical pulses instead of an oscilloscope with a bandwidth of tens of gigahertz.

Note that approximation of the histogram with a half-width of ~80 cm (Fig. 1c) by Gaussian or Voigt curves yields almost identical positions and spreads of the pulse centroid, namely, 31.382 ± 0.007 and 31.377 ± 0.007 m, respectively. This pulse approximation makes it possible, without operator assistance, to increase the accuracy of measurement of the distance to a flat target by a lidar rangefinder to ± 0.7 cm, i.e., by about an order of magnitude with respect to the discretisation step (10 cm) and by two orders of magnitude with respect to the pulse half-width (80 cm).

A photograph of the lidar is given in Fig. 2b; the lidar includes a transmitter/receiver module (weight 240 g) and a control unit (weight 300 g). The lidar was installed in a hot tunnel (Fig. 2b) with a blank wall (43°14′57.7″ N, 42°43′19.5″ E) above the Elbrus volcano magmatic chamber at a distance of 4000 m from the entrance to the Baksan Neutrino Observatory (BNO) tunnel for sensing variations in volcanic aerosol emanation.

The measurements were carried out each 30 min with data acquisition for 100000 lidar pulses. Figure 3 shows typical histograms of a backscattered signal profile without correction for the squared distance from the lidar. The dashed lines confine the regions of summing of photocounts

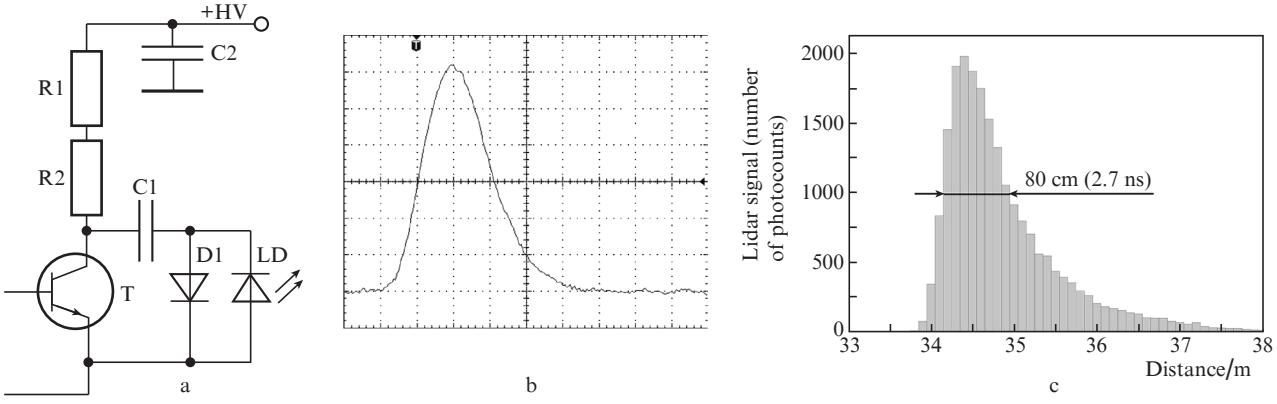

Figure 1. (a) Electric scheme of the end part of the current pulse generator assembled from commercially available discrete elements, (b) laser pulse oscillogram (duration less than 4 ns) on the screen of an Aktakom ADS-2332 oscilloscope with a bandwidth of 300 MHz, and (c) laser pulse in the form of a histogram of lidar photocounts upon sensing a flat wall (resolution 10 cm).

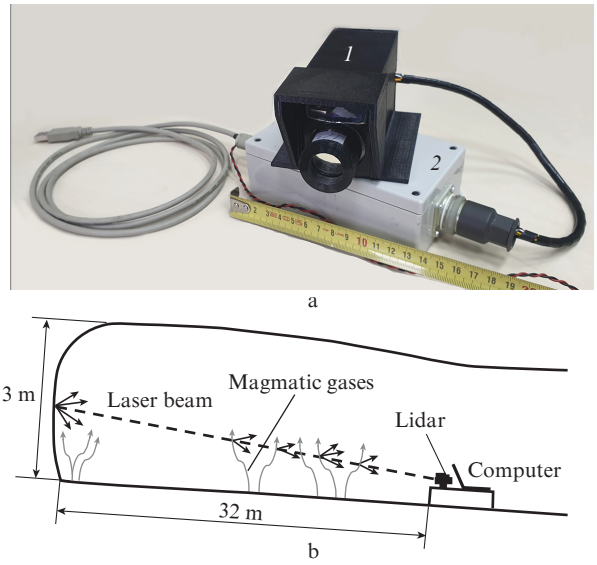

Figure 2. (a) Photograph of the lidar: (*1*) transmitter/receiver module with dimensions of 50 × 60 × 95 mm and a weight of 240 g and (*2*) control unit with a weight of 300 g and (b) scheme of lidar sensing of magmatic aerosols in a hot dead-end tunnel of BNO (longitudinal cross section).

of scattered signals, namely, region 1 corresponds to scattering on aerosols in the tunnel [28.10.2019, curve (*1*) and 29.10.2019, curve (*2*)]; region 2 corresponds to scattering from the blank wall of the tunnel, which reflects variations in the track transmission for the roundtrip (to the wall and back); and region 3 corresponds to the detector noise. One can see that a decrease in the laser pulse duration and an increase in the resolution from 5 m to 10 cm make it possible to detect the modulation of the aerosol scattering profile (region 1).

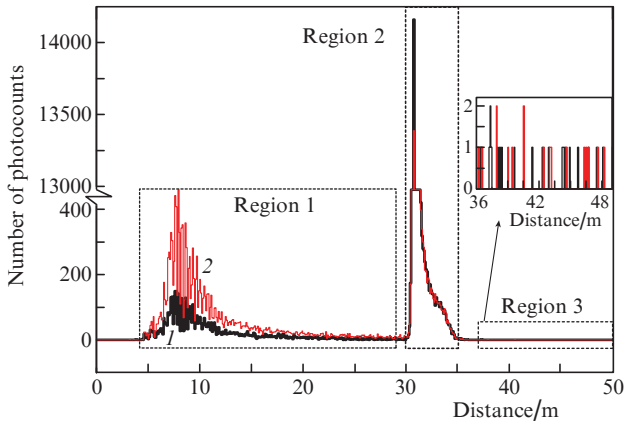

Figure 3. (Colour online) Backscattering profile (number of photocounts) along a tunnel with a discretisation step of 10 cm (*1*) on 28 October 2019, 21:6 UTC and (*2*) 4h after. The dashed lines confine the regions of photocount summation for determining the lidar signals. The inset shows the noise region on a larger scale for better visualisation.

Figure 4a presents the evolution of aerosol emanation in the BNO tunnel from 1 October to 25 December of 2019 [curve (*1*)], the change in the sensing track transmission [curve (*3*)], and the data of the laser strainmeter [20] [curve

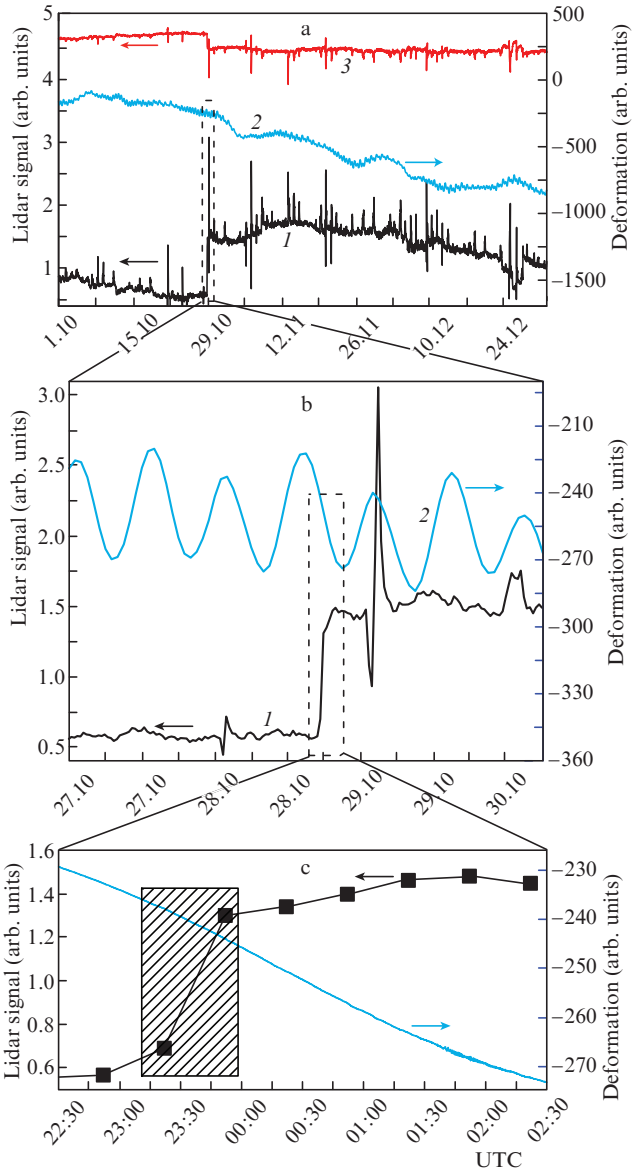

Figure 4. (*1*) Signals of lidar sensing of magmatic aerosol and (*2*) seasonal Earth's crust compression (deformation) determined by a laser strainmeter in the BNO tunnel, as well as (*3*) sensing track transmission per double pass for (a) 1.10.2019–1.12.2019, (b) 27.10.2019–30.10.2019, and (c) 22:30 28.10.2019–02:30 29.10.2019 (the size of squares corresponds to the spread of the lidar data; the dashed rectangle indicates the irreversible jump in the aerosol emanation).

(*2*)]. All measurements were referenced to Coordinated Universal Time (UTC).

Figure 4 clearly shows that the dominant feature is the sharp three-fold increase in the lidar signal. i.e., a 'jump' in the aerosol emanation curve observed for the first time on 28 October 2019. Then, the aerosol scattering signal begins to decrease similarly to the strainmeter signal due to the seasonal compression of hard-rock cracks. Note that the seasonal decrease in the lidar signal (i.e., in aerosol emanation) occurs with the same slope as we measured before the jump.

A rather important factor is that, despite the relatively high resolution ($\sim 1.6 \times 10^{-11}$ m) [20], the laser strainmeter–interferometer with a measuring shoulder 75-m long did not detect noticeable distortions in the interferogram at the instant of jump (see Fig. 4c).

3. Conclusions

Thus, we developed a compact, having no domestic analogues, aerosol lidar based on a short-pulse (3-ns) semiconductor laser with an external current pulse generator assembled from commercially available discrete elements. The laser pulse energy (0.2 μJ at a wavelength of 907 nm) meets the eye safety requirements [6]. The short pulse provides a decimetre resolution of the aerosol lidar and the ability of measuring a 30-m distance with an error of ±7 mm (0.02%). This accuracy is needed to measure the approach and berthing velocities (cm s^{-1}) of large-tonnage space stations. Of particular interest is control of soft landing on planets, as well as of landing of reentry vehicles. The uniquely small weight (540 g) of the lidar allows its positioning on a quadcopter for surface topography and for measuring the height of trees to estimate the ecosystem biomass without specific requirements for eye protection.

Using this lidar, we detected (for the first time to our knowledge) a sharp three-fold increase in aerosol emanation with magmatic gases above the Elbrus volcano magmatic chamber in the BNO tunnel (28 October 2019, 23:00 UTC). It is important that the gas pressure drop and the aerosol emanation jump were not reflected on the signal of a laser strainmeter with a resolution of 1.6×10^{-11} m, which detected the Earth's crust deformation by tidal waves. This means that the lidar based on a short-pulse (3-ns) diode laser is a new highly sensitive detector of geodynamic processes in the family of traditional instruments [20]. However, the nature of the aerosol jump and the gas pressure drop trigger are not yet determined and require a separate investigation.

Acknowledgements. This work was supported by the Russian Science Foundation (Grant No. 19-19-00712).

References

1. Measures R.M. *Laser Remote Sensing: Fundamentals and Applications* (New York: Wiley & Sons, 1984).
2. Bunkin A., Voliak K. *Laser Remote Sensing of the Ocean: Methods and Applications* (New York: Wiley & Sons, 2001).
3. Fiocco G., Smulin L. *Nature*, **199**, 1275 (1963).
4. Veselovskii I.A., Hu Q., Goloub P., Podvin T., Korenskiy M., Pujol O., Dubovik O., Lopatin A. *Atmos. Meas. Tech*., **13**, 6691 (2020).
5. Ceolato R., Berg M.J. *J. Quant. Spectrosc. Radiat. Transf*., **262**, 107492 (2021).
6. Sliney D., Wolbarsht M. *Safety with Lasers and other Optical Sources: A Comprehensive Handbook* (New York: Springer Science & Business Media, 2013).
7. Pershin S.M., Linkin V.M., Makarov V.S., Prochazka I., Hamal K. *Proc. CLEO. Advance Program.* (OSA, 1991) CFI1, p. 120.
8. Prochazka I., Hamal K., Sopko B. *J. Mod. Opt*., **51**, 1289 (2004).
9. Bukharin A.V., Pershin S.M. *Opt. Atm. Okeana*, **7**, 521 (1994).
10. Pershin S. *Proc. Int. Symp. 'Aerospace Sensing'* (Orlando, 1994) Vol. 2222, p. 215.
11. Pershin S.M., Grishin M.Ya., Zavozin V.A., Lednev V.N., Lukyanchenko V.A., Makarov V.S. *Laser Phys. Lett*., **17**, 026003 (2020).
12. Pershin S.M. *Ciência Hoje*, **12**, 71 (1999).
13. https://mars.nasa.gov/internal_resources/818/.
14. Pershin S.M., Dolgikh G.I., Bunkin A.F., Grishin M.Ya., Zavozin V.A., Klinkov V.K., Lednev V.N., Makarov V.S., Plotnikov A.A., Tyurin A.V. *Bull. Lebedev Phys. Inst*., **45**, 214 (2018) [*Kratk. Soobshch. Fiz. FIAN*, **5**, 32 (2018)].
15. Slipchenko S.O., Podoskin A.A., Soboleva O.S., Zakharov M.S., Bakhvalov K., Romanovich D., Pikhtin N.A., Tarasov I.S., Bagaev T.A., Ladugin M.A., Marmalyuk A.A., Simakov V.A. *Proc. SPIE*, **9751**, 97510P-3 (2016).
16. Slipchenko S.O., Podoskin A.A., Golovin V.S., Rastegaeva M.G., Voronkova N.V., Pikhtin N.A., Bagaev T.A., Ladugin M.A., Marmalyuk A.A., Simakov V.A. *IEEE Photonics Technol. Lett*., **33**, 11 (2021).
17. Huikari J., Avrutin E., Ryvkin B., Kostamovaara J. *Opt. Rev*., **23**, 522 (2016).
18. Slipchenko S.O., Podoskin A.A., Soboleva O.S., Pikhtin N.A., Bagaev T.A., Ladugin M.A., Marmalyuk A.A., Simakov V.A., Tarasov I.S. *Opt. Express*, **24**, 16500 (2016).
19. Vainshtein S., Zemlyakov V., Egorkin V., Maslevtsov A., Filimonov A. *IEEE Trans. Power Electron*., **34**, 3689 (2019).
20. Milyukov V.K., Myasnikov A.V. *Meas. Tech*., **48**, 1183 (2005).